Theor Chem Acc (2012) 131:1201
DOI 10.1007/s00214-012-1201-3

REGULAR ARTICLE

Integrated computational approaches for spectroscopic studies of molecular systems in the gas phase and in solution: pyrimidine as a test case

Malgorzata Biczysko · Julien Bloino · Giuseppe Brancato · Ivo Cacelli · Chiara Cappelli · Alessandro Ferretti · Alessandro Lami · Susanna Monti · Alfonso Pedone · Giacomo Prampolini · Cristina Puzzarini · Fabrizio Santoro · Fabio Trani · Giovanni Villani

Received: 24 July 2011 / Accepted: 3 March 2012 / Published online: 8 April 2012

Abstract An integrated computational approach built on quantum mechanical (QM) methods, purposely tailored inter- and intra-molecular force fields and continuum solvent models combined with time-independent and time-dependent schemes to account for nuclear motion effects is applied to the spectroscopic investigation of pyrimidine in the gas phase as well as in aqueous and CCl_4 solutions. Accurate post-Hartree–Fock methodologies are employed to compute molecular structure, harmonic vibrational frequencies, energies and oscillator strengths for electronic transitions in order to validate the accuracy of approaches rooted into density functional theory with emphasis also on hybrid QM/QM′ models. Within the time-independent approaches, IR spectra are computed including anharmonicities through perturbative corrections while UV–vis line-shapes are simulated accounting for the vibrational structure; in both cases, the environmental effects are described by continuum models. The effects of conformational flexibility, including solvent dynamics, are described through time-dependent models based on purposely DFT-tailored force fields applied to molecular dynamics simulations and on QM computations of spectroscopic properties. Such procedures are exploited to

Dedicated to Professor Vincenzo Barone and published as part of the special collection of articles celebrating his 60th birthday.

Electronic supplementary material The online version of this article (doi:10.1007/s00214-012-1201-3) contains supplementary material, which is available to authorized users.

M. Biczysko (✉) · J. Bloino · G. Brancato · G. Prampolini
Scuola Normale Superiore di Pisa Piazza dei Cavalieri 7, 56126 Pisa, Italy
e-mail: malgorzata.biczysko@sns.it

Present Address:
M. Biczysko
Center for Nanotechnology Innovation @NEST, Istituto Italiano di Tecnologia, Piazza San Silvestro 12, 56127 Pisa, Italy

Present Address:
J. Bloino
CNR–Consiglio Nazionale delle Ricerche, Istituto di Chimica dei Composti Organo Metallici (ICCOM-CNR), UOS di Pisa, Area della Ricerca, via G. Moruzzi 1, 56124 Pisa, Italy

I. Cacelli · C. Cappelli
Dipartimento di Chimica e Chimica Industriale, Università degli Studi di Pisa, Via Risorgimento 35, 56126 Pisa, Italy

A. Ferretti · A. Lami · S. Monti · F. Santoro · G. Villani
CNR, Consiglio Nazionale delle Ricerche, Istituto di Chimica dei Composti Organo Metallici (ICCOM-CNR), UOS di Pisa, Area della Ricerca, via G. Moruzzi 1, 56124 Pisa, Italy

A. Pedone
Dipartimento di Chimica, Unversità di Modena e Reggio Emilia, Via G. Campi 183, 41125 Modena, Italy

Present Address:
G. Prampolini
CNR, Consiglio Nazionale delle Ricerche, Istituto per i Processi Chimico-Fisici (IPCF-CNR), UOS di Pisa, Area della Ricerca, via G. Moruzzi 1, 56124 Pisa, Italy

C. Puzzarini
Dipartimento di Chimica "G. Ciamician", Università di Bologna, Via F. Selmi 2, 40126 Bologna, Italy

F. Trani
CECAM, Centre Européen de Calcul Atomique et Moléculaire, EPF Lausanne, Batochime (BCH), 1015 Lausanne, Switzerland

simulate IR and UV–vis spectra of pyrimidine in the gas phase and in solutions, leading in all cases to good agreement with experimental observations and allowing to dissect different effects underlying spectral phenomena.

Keywords Computational spectroscopy · Integrated approaches · QM/MM/PCM · DFT · Post-Hartree–Fock · CCSD(T) · Composite schemes · Hybrid models · Molecular dynamics · Force fields · Time-independent approaches · Time-dependent approaches · Solvent effects · Vertical excitation energies · Electronic spectra · Spectra line-shape · Vibronic transitions · UV–vis · Resonance Raman · Vibrational spectra · IR intensities · Anharmonicity

1 Introduction

Spectroscopy represents a powerful tool for the characterization of molecular systems [1–4]. However, the interpretation of most experimental spectra is difficult due to their inherent complexity caused by thermal or environmental effects and/or to intrinsic properties of the system itself. In this context, computational spectroscopy turned out to be a valuable tool to help unraveling the various contributions to the spectroscopic signal, allowing a better understanding of the underlying phenomena [1, 2, 5–9].

The predictive and interpretative capabilities of computational spectroscopy can be demonstrated by means of quantum mechanical (QM) approaches that nowadays are able to provide results comparable in accuracy to experimental measurements [1, 2, 5, 6, 10–13]. At the state-of-the-art, the most advanced theoretical models are unavoidably restricted to small-sized molecular systems [10–13], mainly because of the high computational cost required to sample the potential energy surface (PES) by means of highly correlated post-Hartree–Fock methods [14]. Currently, the main challenge of computational spectroscopy is the reliable prediction and interpretation of spectra for large molecular systems in complex environments [15–18]. A possible route to obtain accurate results, even for relatively large molecular systems (several dozens of atoms), is provided by hybrid QM/QM′ models [19], which combine less expensive yet reliable electronic structure approaches (e.g., rooted into the Density Functional Theory (DFT)) for the computation of molecular structure, vibrational properties and/or anharmonic force fields (in both ground and excited electronic states) with *a posteriori* refinement of selected properties (harmonic frequencies, relative energies, electronic transitions, etc.) at a higher level of theory. In this respect, we can mention the high accuracy of hybrid coupled cluster (CC)/DFT anharmonic frequencies [20], vibronic energy levels [21] or spin–spin coupling terms [22]. Additionally, even if the implementation of general and efficient computational approaches aimed at the spectroscopic investigation of macrosystems is a very challenging task, appropriate schemes can already be introduced for complex cases, like large flexible biomolecules. An example is provided by the development of *ad hoc* tailored force fields [23–26], which make possible an extensive sampling of the ground and/or excited electronic state PES, combined with *a posteriori* refinements or computation of selected properties on a set of representative configurations [9, 27, 28]. Furthermore, the role of the surrounding environment can be exploited in a time-independent fashion employing the continuum solvation models [29–33], which provide accurate results at a relatively low computational cost [34] and can be combined with several QM models, also including simulations of electronic spectra line-shapes [35–38]. To get a more reliable and quantitative description of the spectral features, considering both electronic and vibrational properties, the basic formulation of continuum models has to be extended beyond the so-called reaction field effects, that is, the direct solvent effect on the molecular wavefunction and the indirect effect on the molecular structure must be accounted for [39–44]. Furthermore, on the basis of the chemical nature of the solute–solvent couple, combined discrete-continuum models, in which a few solvent molecules strongly and specifically interacting with the solute are treated explicitly leading to a sort of supermolecule embedded in a polarizable continuum, can be successfully employed [45–49]. The librational motions of solvent molecules can also be included by means of molecular dynamics or Monte Carlo simulations with explicit solvent approaches [28, 50, 51]. Finally, the molecular system embedded in complex environments can be effectively described by integrated approaches combining advanced quantum mechanics models, density functional theory, molecular mechanics (MM) and the description of environment through polarizable continuum models (PCM) [29–31] leading to the effective QM/DFT/MM/PCM scheme.

In addition to problems related to a reliable description of molecular systems, a direct comparison with the experimental outcomes requires computational tools able to explicitly simulate the spectroscopic features [6]. To this aim, several computational tools, covering a large panel of spectroscopies, in particular those of vibrational and electronic origin, have been developed and coded (see Ref. [44] and [52, 53] for extensive reviews). However, for a broader use of these advanced theoretical models, two key challenges still remain: (1) development of user-friendly yet flexible problem-tailored packages and (2) validation of accurate yet effective computational models, which allow to extend computational spectroscopy studies

to relatively large and complex molecular systems. This paper will present the example of an integrated computational approach for the simulation of IR and UV–vis spectra of a medium-sized dye in the gas and condensed phase. The research field touched by this paper is broad and many scientists have made relevant contributions, as well as several other integrated computational approaches have been worked out in a number of labs all over the world. Therefore, a balanced review of theoretical models and integrated computational approaches for spectroscopy is beyond the possibilities of this work, and we are obliged to refer the interested reader to the broad, existing recent literature, as, for example, Ref. [6, 27, 28, 50, 53–61] and references therein. Here, we make a partial excursus of the field, with the main idea of pointing out a number of key steps that have made possible the building of the specific integrated protocol here presented, following the general idea of developing and validating transferable and user-friendly computational tools. In this context, we will discuss general-purpose approaches aimed at providing computational support for interpreting IR and UV–vis experimental spectra of complex systems, including their environment [8]. These approaches represent a more accurate treatment with respect to the methods still commonly in use in such cases (e.g., harmonic approximation or vertical electronic transitions) and contribute to a better understanding of experimental spectra for the large molecular systems that are routinely studied nowadays. Complementary time-dependent and time-independent routes to simulate spectra will be applied. These allow the evaluation of the line-shapes for vibrational spectroscopy (e.g., infrared) at the anharmonic level and vibrationally resolved electronic spectroscopy (one-photon, electronic circular dichroism). It will be shown that the integration between different computational tools leads to a more complete picture of the overall spectroscopic properties for the system under study, allowing at the same time the validation of computationally affordable approaches and the setup of hybrid schemes that permit accuracy as well as feasibility. The development and validation of such tools should be carried out by comparing results with those obtained from more accurate models and/or with state-of-the-art experimental data. In the present paper, we have chosen, as a test case, pyrimidine, a medium-sized molecule for which investigation by means of highly accurate electronic QM approaches is still feasible. Furthermore, the large amount of theoretical and experimental data available in the literature allows a detailed comparison for various kinds of spectra along with a discussion on the accuracy of the presented computational models. Moreover, being the precursor of nucleobases, pyrimidine is a molecule of general interest, and the present study will provide some additional details to the understanding of its structural and spectroscopic properties.

The paper is organized as follows. First, the computational details and theoretical models of the various approaches used in this work are briefly summarized in the Sect. 2 (a more detailed account can be found in the Supplementary Information (SI)). Next, highly accurate single- and multi-reference post-Hartree–Fock methods are applied to evaluate molecular structure (Sect. 3.1), vertical excitation energies (Sect. 3.2) and harmonic vibrational frequencies (Sect. 3.3) of isolated pyrimidine. These computations, which are among the most accurate theoretical predictions thus far reported, are employed to assess the accuracy of less expensive QM schemes rooted into density functional theory (Sects. 3.1–3.3), which in turn are applied to the time-independent simulation of the vibrational and vibrationally resolved electronic spectra (Sects. 3.3–3.5). The continuum solvent models are discussed in Sect. 3.4 with respect to their applicability to computational spectroscopy and in particular to the specific case of infrared (IR) spectra simulations in solution. In Sect. 3.6, the geometry and Hessian obtained at the DFT level are used to establish system-specific MM force fields employed in classical molecular dynamics (MD) simulations, which allow to account for dynamical and explicit/implicit solvent effects in protic and aprotic media (H_2O and CCl_4, respectively) on the $S_1 \leftarrow S_0$ electronic transition within the time-dependent approach detailed in Sect. 3.7. Finally, the time-dependent (classical) and time-independent (quantum) approaches employed to simulate electronic spectra line-shapes are also compared and their complementarity is pointed out. The examples are chosen to demonstrate the overall good accuracy attainable by such spectroscopic models when used in conjunction with DFT and MM computations. Further possible improvements through adjustments based on more accurate QM computations are also pointed out.

2 Computational approaches

In view of investigating the balance of computational feasibility and accuracy of results as well as to validate effective approaches applicable to large systems, different computational methods have been adopted to explore step by step the accuracy of less demanding approaches with respect to the more accurate (and expensive) ones. Additionally, several time-dependent and time-independent methods that allow to simulate vibrational and/or vibrationally resolved electronic spectra of the isolated molecule as well as of the system embedded in more complex environments have been employed. The focus is here on user-friendly computational approaches implemented in

widely available QM packages or stand-alone codes, which allow effective application for relatively large systems.

2.1 Electronic structure computations

Best estimates of the molecular structure and harmonic force field of pyrimidine in its electronic ground state have been evaluated at the coupled cluster (CC) level of theory by means of composite schemes to account for the incompleteness of basis set and core-correlation effects (see SI section 1.1 for details). The CC singles and doubles approximation augmented by a perturbative treatment of triple excitations [CCSD(T)] [62] has mainly been used in conjunction with the cc-pVnZ [63] basis sets. These calculations have been carried out with the quantum-chemical CFour program package [64].

Post-Hartree–Fock computations of vertical electronic excitation energies have been performed employing the multi-reference second-order diagrammatic perturbation theory (MRPT) in the barycentric Møller–Plesset scheme [65]. The CIPSI algorithm [66, 67] has been applied in order to determine the active space for the configuration interaction (CI) calculations (see SI section 1.2 for details).

The DFT/aug-N07D model [68] developed for spectroscopic studies of medium-to-large molecular systems, which provides an excellent compromise between reliability and computational effort [69, 20], has been used for geometry optimizations, energy, energy gradients and harmonic and anharmonic force field computations in the ground and excited electronic states. Within the DFT approach, the standard B3LYP [70] and its long-range corrected extension CAM-B3LYP [71] functionals and the double-hybrid functional B2PLYP [72] have been employed along with the aug-N07D [73] basis set built from the polarized double-ζ N07D [68] (see SI Section 1.3 for details). All DFT calculations have been performed with the Gaussian suite of quantum chemistry programs [74].

2.2 Force field (FF) development and molecular dynamics simulations

The intramolecular FF parameters for pyrimidine have been obtained with the Joyce [26] program. Details on the FF development and validation can be found in the supplementary information (SI Section 1.4). Classical molecular dynamics simulations of pyrimidine in water and CCl_4 have been performed using both standard periodic boundary conditions (PBC) and the recently proposed general liquid optimized boundary (GLOB) [75, 76] model, an effective hybrid discrete/continuum method for simulating complex systems in soft condensed matter. All simulations have been carried out with the GROMACS software [77] (PBC) and the JERSEY program [78] (GLOB). For both water and CCl_4 solvents, pre-equilibrated solvent boxes have been obtained through preliminary molecular dynamics runs in the NPT ensemble at 298 K and 1 atm, whereas geometry optimizations were performed according to the steepest-descent method [79] (see SI Section 1.5).

2.3 Vibrational spectra computations

Anharmonic vibrational spectra have been calculated by means of the vibrational second-order perturbation theory (VPT2) [80–86], exploiting the fully automated generalized second-order vibrational perturbation (GVPT2) approach [87–89]. The anharmonic force fields have been computed at the DFT/aug-N07D level and additionally, the hybrid CCSD(T)/DFT approach [20, 90, 91] has also been used to evaluate anharmonic frequencies. Concerning the calculation of anharmonic frequencies and intensities in solution, the extension of the GVPT2 model to the polarizable continuum model [92] has been used, and the reported data refer to both the fully equilibrium and the vibrational nonequilibrium solvation regimes [93, 94]. Vibrational harmonic and anharmonic intensities also account for cavity field contributions [43, 95]. For further details, see SI Section 1.6. All VPT2 computations have been performed using a locally modified version of the Gaussian suite of programs [74].

2.4 Electronic spectra simulations

Within the time-independent framework, vibrationally resolved electronic spectra have been simulated through an integrated procedure (described in detail in Ref. [21, 96, 97]) based on the computation of overlap integrals, also known as Franck–Condon (FC) integrals, between the vibrational wavefunctions of the electronic states involved in the transition. Both adiabatic and vertical approaches have been applied to simulate the one-photon absorption (OPA) and the vibrational resonance Raman (vRR) spectra, including the Duschinsky and Herzberg-Teller effects (see SI Section 1.7). Time-independent vibrationally resolved electronic spectra have been computed using locally modified versions of the Gaussian [74] and *FCclasses* [98] programs for OPA and vRR, respectively. They implement an effective prescreening technique of the relevant transitions developed by some of the authors [99]. Alternative routes have been proposed in literature, see for example Ref. [100–102]. In addition, the electronic spectra lineshapes have also been obtained within a time-dependent framework [9, 51] based on classical MD simulations and on-the-fly or *a posteriori* calculation of spectroscopic properties (see SI Section 1.8). Nonspecific solvent effects on the UV-vis spectrum of pyrimidine have been introduced by a

conductor-like polarizable continuum model (CPCM) [103] with vertical excitation energies computed by the linear response LR-PCM/TD-DFT approach [41] within the non-equilibrium regime [104–106].

3 Results and discussion

3.1 The ground-state molecular structure of pyrimidine

The structure of pyrimidine is shown in Fig. 1 along with the atom labeling scheme, while Table 1 summarizes all the geometries obtained in the present work and compares them with experimental data available in the literature [107]. From the given results, it is first observed that frozen-core (fc) CCSD(T)/cc-pVQZ calculations already provide results close to the convergence with respect to the complete basis set (CBS) limit, as the corresponding differences are quite small. The bond lengths decrease by less than 0.002 Å, less than 0.0005 Å for those involving H, and the angles vary by about 0.1° or even less. On the other hand, the reliability of extrapolations carried out employing triple- and quadruple-zeta basis sets has been proven in Ref. [108]. Second, we note that the core-correlation effects are small. Indeed, for angles, the corrections are in all cases smaller than 0.1 degrees, and for bond distances, they amount to about 0.002 Å, about 0.001 Å for bonds involving H. Before proceeding, general considerations on the accuracy of CCSD(T) optimized geometries are warranted. On the basis of the literature available (see for instance Refs. [109, 110] and references therein), the accuracy of CBS+CV structures is expected to be of the order of 0.001–0.002 Å for distances and of about 0.05–0.1° for angles. These are conservative estimates and also account for the approximations made and for neglecting higher-order correlation effects. Concerning the accuracy of the DFT model, on the basis of the comparison reported in Table 1, the conclusion drawn is that both the B3LYP/aug-N07D and CAM-B3LYP/aug-N07D levels provide results of better quality than the CCSD(T)/cc-pVTZ ones. The only exception is given by the C–H bond lengths that result to be too long. The considerations are particularly encouraging as the DFT/aug-N07D approach can be easily applied to compute the structure of significantly large systems (e.g., more than 100 atoms) and then used to develop accurate intramolecular force fields, thus allowing molecular dynamics simulations (*vide infra*). As far as the comparison with experiment is concerned, we first note that the available experimental geometries are partial structures and none of them is an equilibrium structure. In most cases, CBS+CV and experimental values agree within the associated uncertainties. The largest discrepancies are observed for the C_2-C_3 distance for which experiment seems to overestimate the value by about 0.006 Å, and for a few angles in the case of the geometry denoted ED+LCNMR+MW, which is based on electron diffraction and liquid crystal NMR data combined with rotational constants of the parent isotopologue [107].

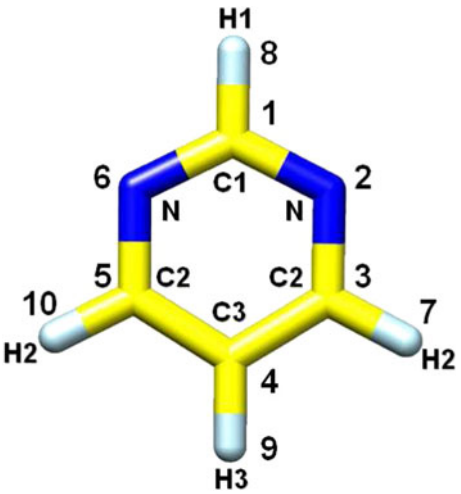

Fig. 1 Geometry and atom numbering scheme employed for pyrimidine

3.2 Post-Hartree–Fock and TD-DFT computation of vertical excitation energies in the gas phase

Energies of the ground and a number of singlet excited electronic states, as arising from excitations in the valence space, have been computed at the best estimated structure of the ground state (see Sect. 3.1 and Table 1). Two different methods have been employed for the vertical excitation (VE) spectrum: the post-Hartree–Fock MRPT method and the popular single-reference time-dependent density functional theory (TD-DFT) approach. For the latter, the CAM-B3LYP [71] functional in conjunction with the aug-N07D [73] and aug-cc-pVQZ [111, 112] basis sets has been used. The choice of functional has been related to its good performance over the large spectra range, as shown, for example, by TD-CAM-B3LYP results for Rydberg and charge transfer excitation energies or static electronic polarizabilities which are notably improved over the standard B3LYP functional [113]. Additionally, both basis sets used for TD-DFT computations include several diffuse functions, thus allowing the representation of a limited number of Rydberg states. In contrast, the MRPT computations have been performed with the 6-311G(d) basis set, and thus, the Rydberg states have not been considered.

In Table 2, the vertical excitation energies obtained from both approaches are compared to the experimental maxima from Ref. [114]. It is apparent that MRPT performs very well for the lowest excited states being

Table 1 Molecular structure of pyrimidine

	CCSD(T)/ cc-pVTZ	CCSD(T)/ cc-pVQZ	CBS	CBS+CV	B3LYP/ aug-N07D	CAM-B3LYP/ aug-N07D	Exp./r_s[a]	Exp./ ED+LCNMR+MW[a]
C_1–N	1.3402	1.3369	1.3351	1.3329	1.3376	1.3310	1.337(2)	1.328(7)
N–C_2	1.3411	1.3380	1.3363	1.3341	1.3386	1.3322	1.332(3)	1.350(7)
C_2–C_3	1.3932	1.3907	1.3891	1.3868	1.3924	1.3861	1.393(2)	1.393(4)
C_1–H_1	1.0837	1.0833	1.0831	1.0820	1.0887	1.0881	–	1.082
C_2–H_2	1.0845	1.0839	1.0837	1.0826	1.0893	1.0884	–	1.082
C_3–H_3	1.0813	1.0808	1.0806	1.0795	1.0856	1.0843	–	1.082
∠N–C_1–N	127.75	127.50	127.37	127.28	127.05	126.89	127.2(3)	128.3
∠C_1–N–C_2	115.36	115.58	115.69	115.75	115.94	116.06	115.8(3)	115.75
∠N–C_2–C_3	122.46	122.36	122.31	122.28	122.23	122.22	122.4(3)	121.2(3)
∠C_2–C_3–C_2	116.60	116.61	116.64	116.65	116.61	116.56	116.4(2)	117.8(2)
∠H_1–C_1–N	116.12	116.25	116.32	116.36	116.48	116.55	–	–
∠H_2–C_2–N	116.38	116.42	116.43	116.46	116.48	116.50	–	–
∠H_3–C_3–C_2	121.70	121.69	121.68	121.67	121.69	121.72	–	120.9(3)

Geometry parameters computed at the coupled cluster and DFT levels of theory and compared with available experimental data

Distances in Å and angles in degrees

[a] Ref. [107]

Table 2 Vertical excitation spectrum as computed at the MR-PT and TD-DFT levels

Assignment	Sym.	MRPT		TD-CAMB3LYP/aug-N07D		TD-CAMB3LYP/aug-cc-pVQZ		Exp.[a]
		E (eV)	f value	E (eV)	f value	E (eV)	f value	E (eV)
$\pi* \leftarrow n_N$	B_1	4.19	0.0042	4.58	0.0062	4.56	0.0053	4.18
$n_N \leftarrow n_N$	A_2	4.59	0.0000	4.94	0.0000	4.93	0.0000	4–5
$\pi* \leftarrow \pi$	B_2	5.16	0.0380	5.85	0.0453	5.84	0.0472	5.22
$\pi* \leftarrow n_N$	A_2	5.68	0.0000	6.03	0.0000	5.99	0.0000	
$\pi* \leftarrow \pi$	B_1	5.99	0.0034	6.33	0.0059	6.30	0.0056	~6
$\pi* \leftarrow \pi$	A_1	7.02	0.0715	6.71	0.0402	6.68	0.0394	6.69
$3s \leftarrow n_N$	B_2			6.86	0.0051	6.82	0.0053	6.42
$3p \leftarrow n_N$	B_1			7.37	0.0175	7.35	0.0160	7.44
$3p \leftarrow n_N$	A_1			7.5	0.2236	7.42	0.1629	6.97
$3p \leftarrow n_N$	B_2			7.56	0.0896	7.48	0.0684	7.05
$\pi* \leftarrow \pi$	A_1	7.79	0.4504	7.63	0.2292	7.58	0.2864	7.48
$\pi* \leftarrow \pi$	B_2	8.13	0.5118	7.84	0.4003	7.81	0.4077	

The oscillator strengths are in the mixed gauge

The experimental vertical transition energies are also reported

[a] From Ref. [114]

competitive with respect to previous calculations performed with the equation-of-motion (EOM)-CC method (see Ref. [114] for extensive review of experimental and theoretical results), whereas TD-CAM-B3LYP overestimates the excitation energies by 0.35–0.7 eV. It should be noted that the TD-CAM-B3LYP/aug-N07D level of theory provides results already converged with respect to the basis set limit, with energies higher than those computed at the TD-CAM-B3LYP/aug-cc-pVQZ level by only ~0.05 eV. The oscillator strengths appear to be systematically higher for TD-DFT although both calculations roughly reproduce the overall experimental optical spectrum. Around 6–7 eV, the TD-DFT spectra include some Rydberg transitions for which intensity borrowing from the most intense transitions occurs. Due to the absence of diffuse functions, no Rydberg transitions are obtained in MRPT calculations. Finally, the very intense $\pi^* \leftarrow \pi$ transition at about 7.5 eV is slightly overestimated by MRPT. The global intensity of these transitions is higher for MRPT because of the intensity borrowing of the TD-DFT transitions to Rydberg

Table 3 Harmonic vibrational frequencies (in cm^{-1}) and IR intensities (in km/mole) computed at the CC and DFT levels

Mode[a]	Sym.	CCSD(T)/ cc-pVTZ		CCSD(T)/ cc-pVQZ		CBS[b]	CBS+CV[c]	B3LYP/ aug-N07D		CAM-B3LYP/ aug-N07D		B2PLYP/ aug-cc-pVTZ	
		ω	Int	ω	Int	ω	ω	ω	Int	ω	Int	ω	Int
1	A1	3,219	7.3	3,217	6.6	3,217	3,223	3,203	9.3	3,230	5.3	3,222	7.9
2	A1	3,189	14.7	3,190	12.7	3,191	3,196	3,175	13.7	3,197	10.5	3,193	12.3
3	A1	3,173	9.4	3,174	9.5	3,175	3,180	3,158	12.7	3,182	12.9	3,178	11.4
4	A1	1,610	32.1	1,613	34.8	1,616	1,621	1,616	47.3	1,659	58.8	1,608	37.6
5	A1	1,425	55.7	1,430	55.6	1,432	1,437	1,437	55.8	1,461	56.3	1,436	57.2
6	A1	1,154	3.0	1,158	2.4	1,160	1,164	1,161	1.3	1,179	0.8	1,161	1.8
7	A1	1,077	1.4	1,079	1.3	1,080	1,084	1,079	1.0	1,095	1.0	1,083	1.0
8	A1	1,001	2.8	1,004	2.8	1,005	1,009	1,013	3.8	1,032	4.4	1,007	3.3
9	A1	684	3.5	686	3.2	687	689	692	3.0	700	3.2	692	2.9
12	B2	3,177	18.5	3,178	15.6	3,179	3,184	3,162	18.1	3,185	14.1	3,181	15.5
13	B2	1,614	72.1	1,616	74.5	1,618	1,623	1,616	84.9	1,659	94.7	1,609	78.0
14	B2	1,493	8.8	1,494	8.1	1,495	1,499	1,495	5.8	1,516	6.4	1,497	5.3
15	B2	1,390	0.3	1,392	0.4	1,392	1,395	1,390	0.3	1,401	0.3	1,400	0.3
16	B2	1,247	6.0	1,248	6.1	1,248	1,253	1,262	3.8	1,271	4.5	1,262	4.7
17	B2	1,193	4.4	1,195	5.4	1,196	1,199	1,228	8.2	1,230	8.4	1,226	7.9
18	B2	1,088	2.0	1,089	1.9	1,088	1,091	1,095	3.1	1,110	2.7	1,094	3.1
19	B2	625	11.5	626	11.4	626	628	634	11.3	641	11.6	631	11.5
20	B1	1,023	0.0	1,024	0.0	1,027	1,031	1,022	0.0	1,047	0.0	1,036	0.0
21	B1	978	0.0	977	0.0	976	980	980	0.1	1,000	0.3	991	0.0
22	B1	819	7.0	818	6.1	817	820	821	5.3	836	5.1	828	6.2
23	B1	732	39.9	732	39.7	731	734	738	41.0	747	42.9	742	39.7
24	B1	350	3.0	349	3.2	349	351	351	3.5	362	3.6	352	3.5
10	A2	1,001	0.0	1,001	0.0	1,001	1,004	998	0.0	1,019	0.0	1,010	0.0
11	A2	402	0.0	403	0.0	403	404	408	0.0	417	0.0	408	0.0

[a] Normal mode numbering as in Ref. [121, 120]

[b] Computations at the (fc)CCSD(T)/CBS level, see text for details

[c] Computations at the (fc)CCSD(T)/CBS+CV(MP2/CVTZ) level, see text for details

states. As far as the excitation spectrum is concerned, on the whole it seems that both methods are able to give reliable results. Concerning TD-B3LYP computations, it has been found that the excitation energies and oscillator strengths for the first two excited electronic states agree very well with MRPT as well as with previous theoretical and experimental data [114] (4.29 eV/0.0047 and 4.62 eV/0.0000, respectively), but, as expected, TD-B3LYP does not provide qualitatively correct results for the energy order and the nature of higher-lying excited electronic states. Thus, for the sake of consistency, the TD-CAM-B3LYP functional has been chosen to compute the electronic spectra line-shapes for all excited electronic states considered in this work; for the six lowest electronic transitions, a hybrid approach with energies corrected by means of the accurate MRPT computations has been used. These results will be discussed in Sect. 3.5, with emphasis on the comparison between experimental and computed band intensities in the 3.5–9.5 eV energy range.

3.3 Vibrational properties of isolated pyrimidine in the ground electronic state

Table 3 summarizes the harmonic frequencies and infrared (IR) intensities obtained at the CC and DFT levels. In regard to CCSD(T) calculations of harmonic frequencies, we note that the (fc)CCSD(T)/cc-pVQZ level of theory already provides converged results with respect to the CBS limit, the differences between CBS and cc-pVQZ being generally smaller than 1 cm^{-1} and being 4 cm^{-1} at most. Core-correlation corrections are in all cases positive (i.e., they enlarge the frequency value) and small (i.e., they range from 1 to 5 cm^{-1}). Moving to IR intensities, it can be noted that also in this case the (fc)CCSD(T)/cc-pVQZ computations are expected to yield results converged with respect to basis set completeness, as the differences between cc-pVTZ and cc-pVQZ are on average of 1 km/mol and not exceeding 3 km/mol. Taking into account that for IR intensities extrapolation schemes have not been

formulated yet and that core-correlation corrections at the MP2/cc-pCVTZ level are smaller than 0.5 km/mol, the (fc)CCSD(T)/cc-pVQZ values can be considered as best estimates for the IR intensities.

The comparison of best theoretical estimates with DFT results confirms the overall good accuracy of the latter. With respect to CC reference values, the B3LYP functional shows a mean absolute error (MAE) of 8 cm^{-1} for frequencies and 2 km/mol for intensities. As already suggested (see Ref. [115, 116]), the accuracy of DFT results is further improved by using the double-hybrid functional B2PLYP and the aug-cc-pVTZ basis set, leading in the present case to a MAE of 6 cm^{-1} for frequencies and showing improvement also for the IR intensities (MAE of 1 km/mol). Thus, B2PLYP computations in conjunction with tiple-ζ quality basis sets can be considered as an alternative to coupled cluster computations in view of improving the accuracy of vibrational properties within hybrid models [20, 115] (*vide infra*). Finally, we also note that the CAM-B3LYP/aug-N07D results show a rather good agreement with the CC reference values (MAE of 16 cm^{-1} for frequencies and 3 km/mol for intensities); therefore, such a level of theory can be applied to cases where long-range effects are important, for example, computations in which both electronic ground and excited states need to be treated at the same time (see Sects. 3.5 and 3.7). Concerning computations beyond the harmonic approximation, it is well recognized that the GVPT2 model applied to anharmonic force fields evaluated at the DFT level (in particular with the Becke-family hybrid functionals, see Ref. [44, 20, 115] for general discussions) and coupled with appropriate criteria to define Fermi [117] and Darling–Dennison resonances is able to provide accurate results for semirigid systems [118]. For pyrimidine, it has been shown that such computations lead to frequencies with an average error with respect to experiment of about 10 cm^{-1} or less [119, 120]. In this work, we emphasize that such an (already good) agreement can be further improved by applying high-level corrections to the harmonic part of the force field.

The anharmonic frequencies computed at the DFT/aug-N07D level and those obtained by means of hybrid CC/DFT schemes are listed in Table 4 and compared to the most recent experimental data by Breda et al. [121], who reported the entire fully resolved Fourier-transform (FT)IR spectra recorded in solid argon. As expected, B3LYP/aug-N07D results show very good agreement with the experiment (MAE smaller than 10 cm^{-1}). Further improvements have been obtained by replacing the harmonic counterpart with the best theoretical estimate. Additionally, the small MAE in the case of hybrid CC/CAM-B3LYP computations points out that the larger discrepancies observed for the CAM-B3LYP itself can be entirely ascribed to the harmonic part of the potential. It should be noted that in the present case, resonant interactions are already well defined at the DFT level; thus, both hybrid approaches (see SI Section 1.6), the *a posteriori* one ($\omega_{CC}+\Delta\nu_{DFT}$) and the so-called *direct* model (ω_{CC}/K_{DFT}), lead to similar improvements over DFT results (for explanation of $\omega_{CC}+\Delta\nu_{DFT}$ and ω_{CC}/K_{DFT} models, see SI Section 1.6). In general terms, the *direct* model is necessary when harmonic DFT force field either gives an incorrect prediction of resonant terms or shows large inaccuracies. Computational results have also been used to simulate IR spectra line-shapes (convoluted with Gaussian functions with an half-width at half-maximum (HWHM) of 1 cm^{-1}) directly comparable with the experimental FTIR ones [121] (see Fig. 2). For such comparison, the theoretical spectrum beyond the harmonic approximation also includes overtones and combination bands, whose intensities have been evaluated from DFT GVPT2 computations, while intensities of fundamental bands have been evaluated through the hybrid CC/DFT *a posteriori* scheme. It is evident that anharmonic corrections to both vibrational frequencies and intensities are necessary to correctly reproduce the experimental outcomes; they are thus recommended for an unequivocal analysis and assignment of experimental spectra. The conclusion that can be drawn from this section is that the hybrid models presented in this work are cost-effective approaches to simulate vibrational spectra, which combine the feasibility of accurate harmonic frequency computations with the possibility of properly accounting for vibrational effects beyond the harmonic approximation. In this respect, the CC/B3LYP approach can be applied to systems with up to 10–15 atoms, while the B2PLYP/B3LYP one allows extension toward larger systems of biological and/or technological interest.

3.4 Vibrational anharmonic spectra of solvated pyrimidine: time-independent approach

Due to the availability of analytical expressions of the energy second derivatives, the harmonic oscillator/rigid rotor model can be nowadays routinely applied to solvated systems treated within continuum solvation models, giving reasonably accurate results and reproducing the main features of vibrational spectra of systems in solution [43, 44, 92, 93]. However, methods for evaluating anharmonic effects on vibrational frequencies of solvated systems are still in their infancy, with only few attempts reported in the literature so far [42, 92, 93]. In this view, recent papers by some of the authors [92, 93] have reported promising results, showing that both the accuracy and the scaling characteristics of the corresponding computations in vacuum can be retained for both IR frequencies and intensities. Before discussing the results of the application of the

Table 4 Anharmonic vibrational frequencies of pyrimidine obtained from GVPT2 computations with the semi-diagonal quartic force fields evaluated at the DFT and hybrid CC/DFT levels (see SI, Section 1.6 for details) and compared to the most recent experimental data (FTIR spectrum of pyrimidine isolated in solid argon form Ref. [121])

Mode[a]	Sym.	Assignment[b]	B3LYP/aug-N07D			CAM-B3LYP/aug-N07D			Exp[c]
			DFT	$\omega_{CC}+\Delta\nu_{DFT}$	ω_{CC}/K_{DFT}	DFT	$\omega_{CC}+\Delta\nu_{DFT}$	ω_{CC}/K_{DFT}	ν
1	A1	ν_{C3H3}	3,055	3,074	3,072	3,089	3,081	3,075	3,091.4
2	A1	ν_{C1H1}	3,053	3,074	3,073	3,050	3,049	3,074	3,057.4
3	A1	ν_{CH}sym	3,030	3,052	3,051	3,075	3,073	3,051	3,041
4	A1	ν_{CC}sym + ν_{CN}sym	1,573	1,578	1,578	1,616	1,579	1,576	1,567.3
5	A1	δ_{CH}sym + ν_{CN}sym	1,408	1,408	1,408	1,433	1,409	1,408	1,400.6
6	A1	ν_{CN}sym + δ ring	1,141	1,145	1,143	1,161	1,146	1,150	1,138.2
7	A1	ν_{CC}sym + δ ring	1,053	1,057	1,074	1,070	1,059	1,072	1,070.7
8	A1	δ ring + ν_{CN}sym	997	993	993	1,017	993	992	989.5
9	A1	δ ring	683	680	680	692	681	680	677.7
12	B2	ν_{CH}as	3,033	3,055	3,054	3,055	3,054	3,053	3,052.1
13	B2	ν_{CC}as + ν_{CN}*as*	1,557	1,564	1,562	1,615	1,579	1,562	1,570.5
14	B2	δ_{CH}	1,463	1,467	1,467	1,486	1,468	1,467	1,464.8
15	B2	δ_{CH}	1,362	1,367	1,366	1,373	1,367	1,367	1,374
16	B2	ν_{CN} + δ_{CH}	1,228	1,220	1,220	1,245	1,227	1,224	1,223.2
17	B2	ν_{CN}as + ν_{CC}*as*	1,197	1,167	1,170	1,197	1,166	1,163	1,156.8
18	B2	δ_{CH}	1,075	1,072	1,072	1,091	1,073	1,072	1,073.9
19	B2	σ ring	626	621	621	634	621	621	620.9
20	B1	γ_{CH}sym	1,002	1,010	1,011	1,024	1,008	1,008	
21	B1	γ_{CH}	958	958	959	979	958	957	
22	B1	τ ring + γ_{CH}	807	806	806	820	805	804	803.1
23	B1	τ ring + γ_{CH}	723	719	719	731	718	717	719.2
24	B1	τ ring	344	343	343	354	342	342	
10	A2	γ_{CH}as	979	985	985	998	983	982	
11	A2	τ ring	400	396	396	409	396	396	
MIN[d]			−36	−17	−20	−7	−12	−17	
MAX[d]			40	16	15	49	32	17	
MAE[d]			11	7	6	19	7	6	

[a] Normal mode numbering as in Ref. [120, 121]

[b] Assignment from Ref. [121] based on the potential energy distribution (PED) analysis, checked through visual inspection of atomic displacements along normal modes

[c] Ref. [121]

[d] Mean absolute error (MAE), and largest negative (MIN) and positive (MAX) deviations with respect to experiment

newly formulated PCM for anharmonic spectra of solvated systems (see Refs. [92, 93]), it is worth recalling some basic concepts. The formulation of a physically consistent continuum model to treat IR intensities in solution requires to consider that formally the "local field" acting on the solute does not coincide to the external field applied to the system, as in the case for the isolated molecule. However, the response of the molecule in the cavity within a dielectric medium depends on the field locally acting on the molecule in the cavity, so that, as already pointed out in the literature [43, 44, 93], in order to gain a reliable connection between the microscopic properties of the molecule and the macroscopic response, it is compulsory to account for the difference between the Maxwell and cavity fields. In addition, due to the fact that spectroscopic properties are by definition time-dependent phenomena (due to the oscillatory nature of the radiation field), a time dependence has also to be taken into account in the definition of the solvation model. In the field of IR spectroscopy, the time dependence of the radiation field is to be considered in the formulation of the cavity field, which is reflected in a proper definition of the dielectric permittivity. However, in the case of an oscillatory motion caused by an external electric field on a molecule surrounded by a dielectric

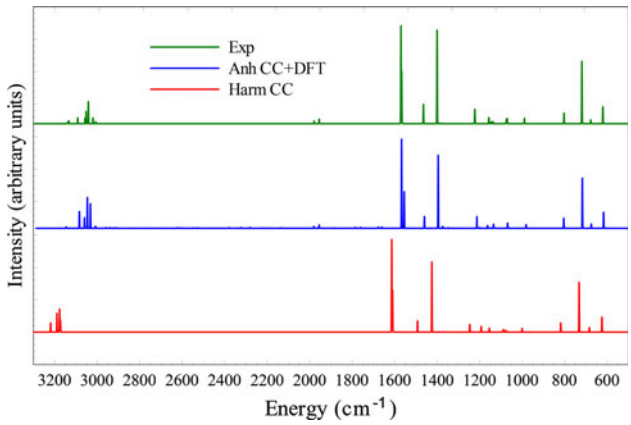

Fig. 2 Computed and experimental [121] IR spectra of isolated pyrimidine. IR spectra *line*-shapes have been convoluted with Gaussian functions with a HWHM of 1 cm^{-1}

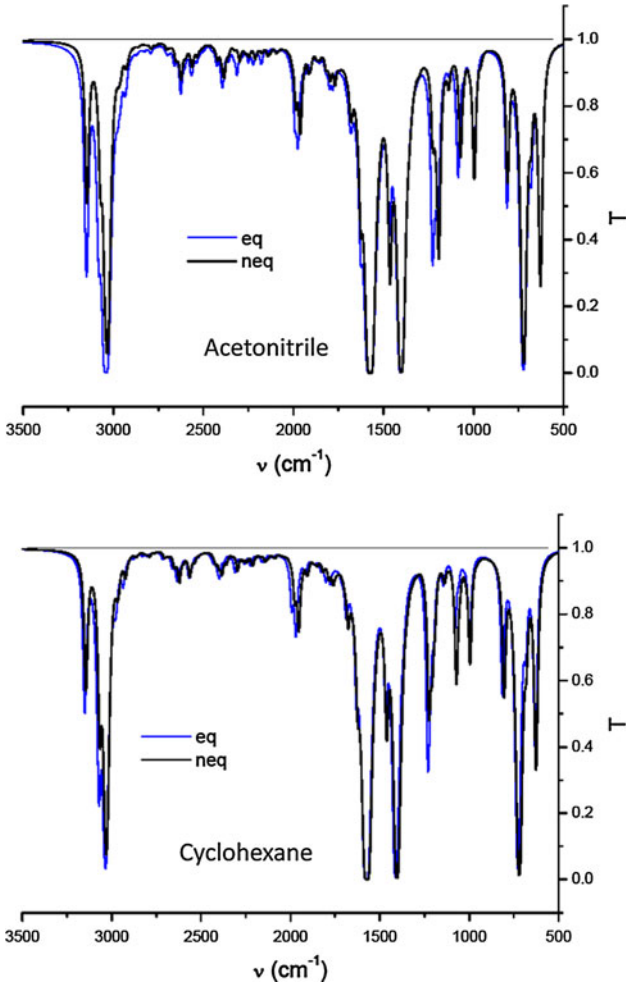

Fig. 3 Calculated IR spectra of pyrimidine in acetonitrile (*top*) and cyclohexane (*bottom*). IR spectra *line*-shapes have been convoluted with Gaussian functions with a HWHM of 2 cm^{-1}

medium, the definition of the solvent response is different whether the solvent nuclear and electronic distributions are assumed to instantaneously rearrange to follow the oscillating molecule (vibrational equilibrium solvation regime) or there exists some dephasing between the solute and the solvent motions (vibrational nonequilibrium solvation regime), so that the solvent distribution is only partly equilibrated to the oscillating molecule. Nonequilibrium effects are most usually addressed in the field of electronic phenomena (electronic excitations, emission or electronic response properties), for which there is a wide literature published in the field [39, 40]. Less standard and much less studied is the consideration of solvent nonequilibrium effects connected to the vibration of a solute surrounded by a continuum dielectric. In the latter case, in fact, to the best of our knowledge, only the contributions given to the groups of Rivail et al. [42] (limited to harmonic frequencies only) and Tomasi et al. [94] (addressing harmonic IR frequencies and intensities [94], Raman activities [122] and VCD rotational strengths [123]) were present in the literature before the recent extensions to treat IR frequencies and intensities beyond the harmonic approximation [93]. Back to pyrimidine, anharmonic GVPT2 vibrational frequencies and the deperturbed (DVPT2) IR intensities computed in the gas phase and CS_2 solution are compared in Table 5, clearly showing that the solvent effect cannot be simulated through simple scaling of gas-phase frequencies and intensities. For instance, the frequency of the ν_4 mode is only little affected by the solvent, while its intensity computed within the nonequilibrium regime is enhanced by more than 15 km/mol. Another example is provided by the ν_{13} mode, as its frequency increases by more than 10 cm^{-1} in solution (neq. regime), while its intensity remains almost unaffected.

More detailed insights on solvent effects and on the differences between the equilibrium and nonequilibrium regimes are provided by the simulated anharmonic spectra shown in Fig. 3 for pyrimidine in cyclohexane and acetonitrile solutions in the 500–3,500 cm^{-1} range. The usual equilibrium approach and the full vibrational nonequilibrium model are compared: in both cases, cavity field effects are included, so that the IR intensities obtained are directly comparable to experimental findings. In addition, not only fundamentals, but also overtones and combination bands are reported. In general, the frequencies of the various bands are quite similar, irrespective of the solvent and of the solvation regime assumed (although nonequilibrium values tend to be slightly higher in frequency). A notable difference is instead noticed for intensities (which are reported as transmittance values, as it is common in the IR spectroscopy): not only absolute values, but especially relative intensities differ remarkably by changing the solvating environment, and for a given solvent, moving from

Table 5 Anharmonic vibrational frequencies (cm^{-1}) and IR intensities (km/mol) of isolated pyrimidine and in CS_2 solution

Mode[a]	Sym.	gas phase		CS_2 eq.		CS_2 neq.	
		v	Int	*v*	Int	*v*	Int
1	A1	3,055	14.7	3,073	16.0	3,066	7.1
2	A1	3,053	6.9	3,047	2.5	3,042	1.7
3	A1	3,030	22.3	3,034	20.1	3,028	15.9
4	A1	1,573	80.9	1,577	82.3	1,573	96.7
5	A1	1,408	55.5	1,412	69.1	1,402	77.1
6	A1	1,141	1.4	1,145	0.8	1,136	1.2
7	A1	1,053	1.1	1,059	0.6	1,052	0.0
8	A1	997	4.0	999	3.9	996	5.8
9	A1	683	2.9	684	3.1	680	2.1
12	B2	3,033	23.1	3,039	22.0	3032	12.4
13	B2	1,557	43.6	1,574	43.5	1,569	43.7
14	B2	1,463	5.6	1,468	6.2	1,461	9.1
15	B2	1,362	0.1	1,371	1.8	1,359	0.1
16	B2	1,228	6.5	1,232	14.2	1,223	8.3
17	B2	1,197	6.0	1,200	3.5	1,191	0.4
18	B2	1,075	3.6	1,082	3.1	1,071	6.8
19	B2	626	11.7	631	12.5	626	14.5
20	B1	1,002	0.0	1,010	0.0	1,000	0.0
21	B1	958	0.1	965	0.0	956	0.1
22	B1	807	5.5	816	7.5	805	7.2
23	B1	723	40.6	728	47.7	719	63.1
24	B1	344	3.5	347	3.7	340	5.4
10	A2	979	0.0	988	0.2	979	0.0
11	A2	400	0.0	402	0.0	397	0.0

For CS_2 solution, the PCM approach within equilibrium (eq.) and nonequilibrium (neq.) models has been applied. All computations at the B3LYP/aug-N07D level

[a] Normal mode numbering as in Ref. [121, 120]

equilibrium to nonequilibrium. Furthermore, the whole solvent effect and the nonequilibrium component do not act homogeneously on each band; therefore, the reported spectra cannot simply be obtained through a scaling procedure (see also Table 5) as bands intensities may be differently affected by changes in the solvating environment. Such a feature of the PCM model (i.e., the different effects on each vibrational mode) is strictly connected to the definition of the cavity, of molecular shape. Thus, the actual geometrical properties of the molecular system under study come into play, as it is physically consistent. Such a characteristics is already included in some continuum solvation models [31–33], but several others based on a spherical description of the molecular cavity [43, 44] are still used to analyze solvent effects on experimental vibrational spectra. In order to get a better insight into the reliability of the results computed with the PCM, calculated and experimental spectra are compared in Fig. 4. In this case, computed values refer to a CS_2 solution of pyrimidine, while experimental data [124] refer to a solution 10 % in CCl_4 for the 3,800–1,370 cm^{-1} range, and 10 % in CS_2 for the 1,370–450 cm^{-1} one. Due to the small difference in the dielectric properties of CS_2 and CCl_4, the calculations have only been performed in CS_2. On the whole, the experimental spectrum is well reproduced. A small shift in frequency absolute values is observed, which is of the same order as those associated with the B3LYP/aug-N07D GVPT2 computations in the gas phase. As far as intensities are concerned, the relative values are reliably reproduced, and notably, a good accuracy is reported for the 2,000–3,000 cm^{-1} spectra range, where anharmonicity plays a substantial role.

3.5 Vibrationally resolved electronic absorption and resonance Raman spectra of isolated pyrimidine, adiabatic and vertical time-independent models

3.5.1 One-photon absorption spectra

Pyrimidine S_0 equilibrium structure belongs to the C_{2v} symmetry point group. The first excited state S_1 belongs to the B_1 irreducible representation (irreps) in C_{2v}, and its PES presents a saddle point, with an imaginary frequency

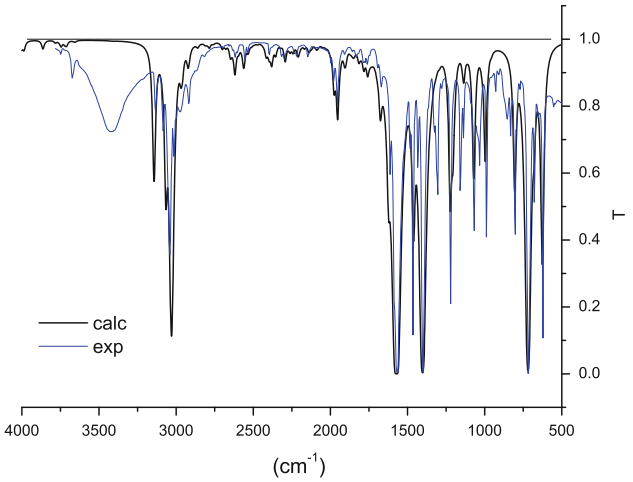

Fig. 4 Calculated versus experimental IR spectrum of pyrimidine in CS_2 solution. IR spectra *line*-shapes have been convoluted with Gaussian functions with a HWHM of 2 cm^{-1}. The experimental spectrum is taken from NIST [124] and refers to a solution 10 % in CCl_4 for 3,800–1,370 cm^{-1}, and 10 % in CS_2 for 1,370–450 cm^{-1} and has a resolution of 2 cm^{-1}

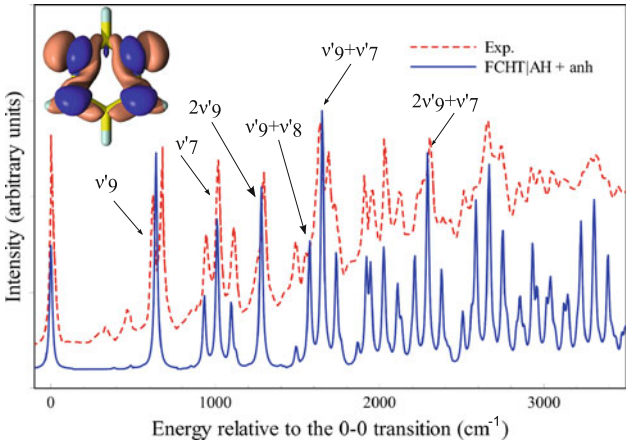

Fig. 5 Computed and experimental [114] spectra for the $S_1 \leftarrow S_0$ electronic transition of isolated pyrimidine, along with the assignment of the most intense vibronic bands. Both spectra are reported with the corresponding 0–0 transition energy set to 0. The theoretical spectrum has been simulated with the Gaussian function with HWHM of 10 cm^{-1} and corrected for anharmonicity though effective scaling procedure using the best CC/B3LYP estimates for the electronic ground-state frequencies. Electron density difference is also plotted (with isovalue of 0.002); regions that gain electron density upon $S_1 \leftarrow S_0$ transition are shown as dark blue, while regions that loose electron density are presented in light coral

of *i*440 cm^{-1}, along a b_2 mode ($Q_1^{(C_{2v})}$), roughly corresponding to the ground-state normal mode of ν_{17}). Distorting the geometry along such a mode, two degenerate global minima arise in C_s symmetry, with S_1 belonging to the A'' irreps. These features point out the existence of an inherently anharmonic double-well energy profile. Therefore, an accurate calculation of the $S_1 \leftarrow S_0$ absorption spectrum should require a full anharmonic treatment of both eigenenergies and eigenfunctions of S_1 vibronic levels [125], but such a challenging treatment is beyond the illustrative scopes of the present contribution. It has been postulated that, also in the presence of such a double-well profile, a harmonic description of the spectrum obtained building the harmonic PES from the Hessian computed at the saddle-point structure, and assigning a convenient real frequency to the imaginary-frequency mode, may deliver useful information and provide spectra in nice agreement with the experiment, provided that the main focus is on low-resolution spectra and/or high-frequency progressions [126]. The reliability of such a model is even improved when the energy barrier of the double-well is so small that no vibrational states are actually confined in the wells, since in that case anharmonic wavefunctions closely resemble the harmonic ones, once associated with a suitable "effective" frequency. In the specific example of the S_1 state of pyrimidine, the saddle point is only 71 cm^{-1} above the global minima. Furthermore, the $Q_1^{(C_{2v})}$ mode is projected on about ten normal modes of the C_s structure, with the largest projection being about 0.5 on a mode $Q_3^{(C_s)}$ with a frequency of 460 cm^{-1}. It can be, therefore, guessed that no vibrational states are confined in the C_s wells, since even the ground state along mode $Q_1^{(C_{2v})}$ has enough energy to overcome the barrier. This case should, therefore, fall in the category mentioned above, and a harmonic PES model with a minimum in the C_{2v} saddle-point structure should deliver rather reliable spectra. The nice agreement between simulated and experimental spectra shown in Fig. 5 confirms *a posteriori* this assumption and allows a more detailed analysis of experimental outcomes. The analysis of individual vibronic transitions points out that the most intense absorptions correspond to the in-plane ring deformations of A_1 symmetry which, due to a small Duschinsky mixing, are well described by their ground-state counterparts (ν_9',ν_8' and ν_7'). These results only partially agree with the experimentally proposed assignment, for example, suggesting that the band at about 3.98 eV is related to the ν'_7 fundamental rather than to some overtone transition. The detailed assignment analysis is beyond the scope of present, illustrative work, and thus has been postponed to future investigations. Concerning the nature of above mentioned energy barrier it can be observed that moving from C_{2v} to C_s stationary points, the *x* component of the S_1 transition dipole moment, perpendicular to the molecular plane, decreases from 0.29 to 0.16 Debye, while for S_2 (A_2 in C_{2v} and A'' in C_s), it increases from 0.0 to 0.15 Debye. This behavior strongly suggests that the S_1 and S_2 states couple when the geometry is distorted to C_s (where both belong to the same irreps), thus exchanging transition intensity with *x*-polarization. Symmetry arguments indicate

that the B_1 and A_2 states can be coupled by movements along b_2 modes ($A_2 \otimes b_2 = B_1$). It is, therefore, reasonable that the S_1 double-well along $Q_1^{(C_{2v})}$ b_2 mode actually arises from the B_1/A_2 nonadiabatic coupling. However, the energy gap between these two states is about 0.4 eV at the Franck–Condon point, thus suggesting that at least the low-energy wing of the spectrum can reasonably be computed through adiabatic approaches like those adopted here [52].

According to our calculations, frequency changes and Duschinsky mixings blue-shift the first-moment (i.e., the center of gravity (CoG)) of the spectrum with respect to the vertical transition energy (VE) by about 0.03 eV, while the shift increases to about 0.04 eV if the Herzberg-Teller (HT) effect is also considered. Since CoG is strictly related to the maximum of the low-resolution absorption spectrum, being identical to the latter for symmetric line-shapes, and somewhat blue-shifted for asymmetric line-shapes, the present analysis allows a number of interesting considerations. First, the small deviation from CoG and VE confirms that very good agreement between MRPT VE and experimental band maximum is not biased by neglecting vibronic contributions. Second, the fact that HT effects blue-shift the CoG by only 0.01 eV supports the reliability of classical simulations of the spectrum (reported in following sections), even for the $S_1 \leftarrow S_0$ transition, for which the existence of HT effects would pose an additional challenge to such a classical treatment [127].

The application of the simplified vertical gradient (FC|VG) model to simulate the electronic spectra of pyrimidine in a broader energy range, covering several electronic transitions, has been validated by the comparison with simulated FCHT adiabatic Hessian (FCHT|AH) and experimental spectra [114] for the $S_1 \leftarrow S_0$ electronic transition (see SI, Figure 1). It is clear that such a simple single-state approach does not allow to take into account all possible effects influencing the spectral phenomenon (such as the nonadiabatic and anharmonic ones). Nevertheless, it should be noted that the FC|VG model usually allows to simulate qualitatively correct spectrum line-shapes even in broad energy range, encompassing several electronic transitions, as in the present case, for which TD-CAM-B3LYP inaccuracies in prediction of absolute VE have been overcome by applying the hybrid MRPT/DFT approach. Figure 6 documents in fact a remarkable agreement of the computed and experimental spectra in the whole energy range, especially if one considers that the most significant discrepancy, namely the underestimation of the relative intensity of the red-shoulder at about 6.7–7 eV with respect to the major band at $\sim$7.5 eV, is probably connected to the fact that vibronic borrowing mechanisms, like HT and nonadiabatic effects, have not been included in the present simulation.

3.5.2 *Resonance Raman spectra*

To complete our analysis, we also report the theoretical vibrational resonance Raman (vRR) spectrum of pyrimidine in water solution for an incident frequency in resonance with the $S_1 \leftarrow S_0$ transition. Figure 7 shows the vRR spectrum for an incident frequency equal to the VE

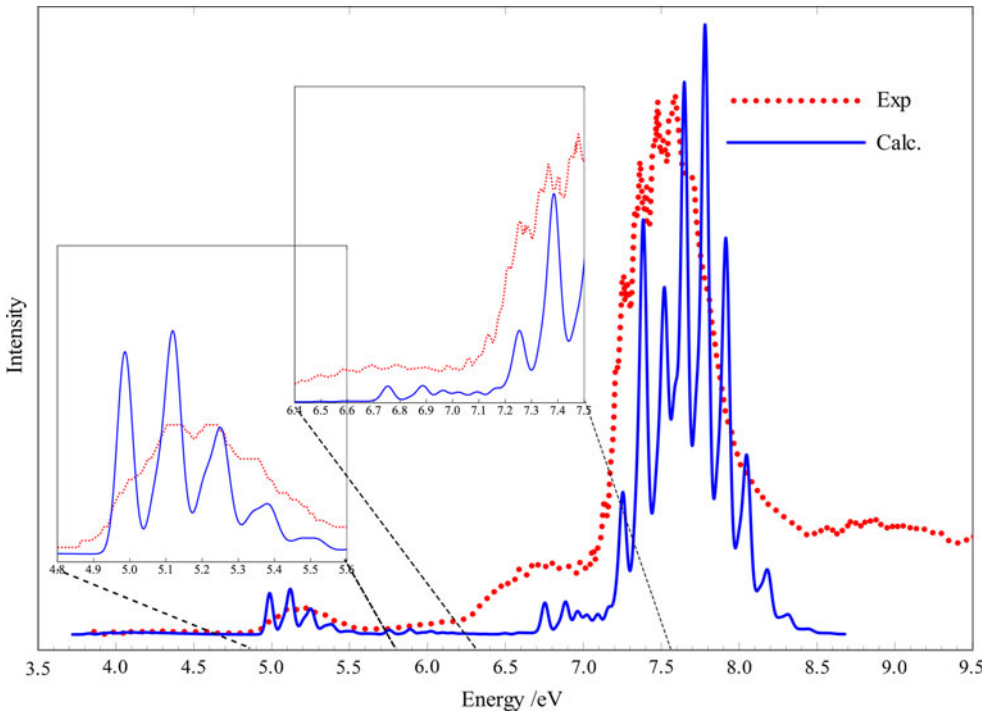

Fig. 6 Theoretical and experimental spectra [114] of isolated pyrimidine in the 3.5–9.5 eV energy range. Absorption spectrum has been computed at the FC|VG level, applying the hybrid MRPT/DFT approach (see text for the details). The theoretical spectrum has been simulated with the Gaussian function with HWHM of 0.025 eV

according to different models, namely Franck–Condon adiabatic shift (FC|AS), FC|AH and FCHT|AH. We assumed a linewidth for the S_1 excited state of 0.05 eV, and we broadened the peaks along the Raman shift coordinates with a Gaussian with HWHM = 25 cm^{-1}. Unfortunately, to the best of our knowledge, no experimental data for such a spectrum have been reported in literature till now, and it is not, therefore, possible to check the reliability of our predictions. Nonetheless, interesting features can be highlighted. In fact, the comparison of FC|AS and FC|AH spectra indicates that the effect of Duschinsky mixings and frequency changes in S_0 and S_1 introduces only modest changes in the spectrum, where all the dominant lines arise from fundamentals of total symmetric a_1 modes, and a few overtones (see the $2\nu_7'$ transition). As expected from the weakness of the resonant transition (nπ^*), inclusion of HT effects has a strong impact on the spectrum. Besides a general enhancement of most of the peaks (observed also for OPA), new bands, absent in the FC spectra, arise. The most intense new bands are the fundamentals of b_1 (ν_{24}' and ν_{22}') and a_2 (ν_{10}', though hidden below the $1\nu_8'$ line) modes, while interestingly the overtone of the latter is also seen in the FC spectrum, due to the very strong frequency changes between the two states ($\sim$450 cm^{-1}). Symmetry considerations show that the S_1 (B_1) state can couple with A_1 states through distortions along the b_1 modes, borrowing z-polarized component of the transition dipole moment (TDM). Distortions along a_2 modes lead to S_1/B_2 coupling, with the latter gaining a y-polarized component of the TDM. Inspection of Table 2 shows that the first A_1 and B_2 symmetry states are actually the strongest OPA absorbers up to the sixth electronic state.

The 2D vRR spectrum, computed according to the method in Ref. [97], is shown in SI Figure 2, where for better visualization, the Raman shift interval has been reduced with respect to what appears in Fig. 7. Such 2D spectra provide a full picture of the resonance scattering phenomenon. It is interesting to notice that the so-called Raman excitation profiles (provided by 1D cuts of the 2D spectrum at fixed Raman shifts) show a clear dependence on the specific vibrational transition under analysis.

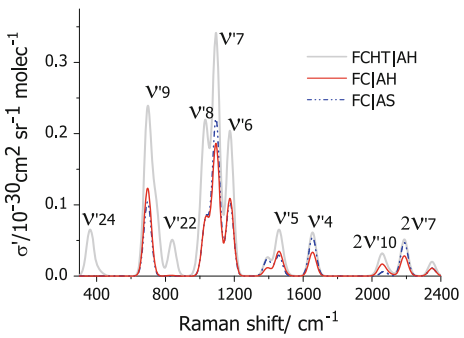

Fig. 7 Vibrational resonance Raman spectrum from the ground vibrational level of S_0, for an incident frequency corresponding to the $S_1 \leftarrow S_0$ vertical transition

3.6 Molecular dynamics simulations

Two separate sets of MD runs have been performed for pyrimidine in water and CCl_4 solvents, using the DFT-tailored FF's. For each solvent, after a 2.5 ns equilibration, a 3 ns production run has been carried out, saving the trajectories every 0.5 ps. It is worth noting that, as expected, no significant differences in the microsolvation of pyrimidine in aqueous solution have been observed between the GLOB and PBC MD simulations, thus validating the physical consistency of both approaches in the present case. Therefore, in the following, we report only the results obtained with the latter methodology. Before running MD simulations in solvent, a preliminary validation of the parameterized FF has been performed by vibrational harmonic frequency computation and MM geometry optimization, combined with *a posteriori* evaluation of UV-vis absorption spectra *in vacuo* at the TD-CAM-B3LYP/aug-N07D level of theory. The quality of the developed FF is illustrated by comparing the FF vibrational harmonic frequencies with those obtained from CAM-B3LYP/aug-N07D calculations (the reference for the FF development) as well as with the best theoretical estimates computed at the CC level. As shown in Fig. 8, the overall agreement is rather good, in particular, in view of the good match with the CC data. Moreover, all pyrimidine internal coordinates (IC's), obtained through geometry optimization at MM and QM levels, agree within a maximum error of 0.03 Å, 0.4° and 0.6° for bonds, angles and dihedrals, respectively (see SI, Table 2). Additionally, since even small geometrical differences can induce

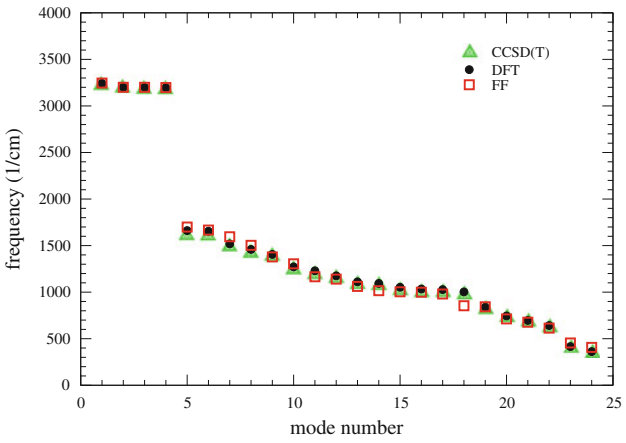

Fig. 8 CCSD(T) (*triangles*), DFT (*full circles*) and FF (*empty squares*) harmonic vibrational frequencies after Joyce parameterization

nonnegligible shifts on the spectroscopic properties, the overall good agreement between energy and oscillator strength computed for the first 10 excited states at both DFT and MM optimized geometries is noteworthy (see SI, Table 3). Further details on FF validation are gathered in SI Section 1.4.

3.6.1 Water

Structural characterization of the solvation shells around pyrimidine has been performed by the analysis of the N–O_W, N–H_W and $CM_{pyrimidine}$–CM_{H2O} radial distribution functions (RDF's), which are reported in Fig. 9 and complemented by spatial distribution functions (SDF). As it appears from the examination of the SDF contours in water (red and cyan surfaces represent oxygen and hydrogen atoms, respectively), a strong clustering of the solvent molecules takes place near pyrimidine nitrogen atoms, which are engaged in quite stable and persistent intermolecular hydrogen bonds with water molecules. The percentage of occupancy of these specific interactions is about 98 %, which means that pyrimidine nitrogens are in contact with water for the whole simulation time. Also, the average number of hydrogen bonds (HB) between pyrimidine and water is about 3, where the largest amount comes from the pyrimidine nitrogens acting as hydrogen bond acceptors (about 1.3 HB for each nitrogen) plus a very small contribution from all the other hydrogen bonding forms. Note that hydrogen bonds were determined based on cutoffs for the donor–hydrogen–acceptor angle (60°, 0° corresponding to the linear donor–hydrogen–acceptor arrangement) and the hydrogen-acceptor distance (2.5Å). Such an hydrogen bonding pattern is also represented by the radial distribution functions where two sharp peaks are observed at 1.8 and 2.8Å in the $g(N\cdots H_W)$ and $g(N\cdots O_W)$ profiles, respectively (see Fig. 9).

The number of solvent molecules within 2.5 and 5.5 Å of at least one pyrimidine atom and in the shells between 2.5 and 3.5 (*sh*2), 3.5 and 4.5 (*sh*3), 4.5 and 5.5 Å (*sh*4) has also been monitored. The distributions of this solvation number are displayed in SI, Figure 4 and further support the conclusion drawn from RDF analysis. The most probable situation is to have 5 waters in the first solvation layer, where at least two of them are hydrogen bonded to the two pyrimidine nitrogens. Moreover, *sh*2 and *sh*3 are equally populated (14 waters), *sh*4 is filled with 20 waters on average, and 52 water molecules are found within 5.5 Å from at least one atom of the solute.

These data can be compared with those reported in Ref. [128], where a combined Monte Carlo-QM approach was carried out to study the solvatochromism of pyrimidine in water and carbon tetrachloride. Note that, apart small changes in the intermolecular FF parameters, the major difference with Ref. [128] is the (intra) molecular flexibility included through the JOYCE procedure in this work, while in Ref. [128], both solvent and solute molecules were kept rigid. It should be stressed that this approximation holds for fairly rigid molecules (like pyrimidine) but may cause large errors when applied to larger flexible molecules (see for instance Refs. [129, 130]). Despite the aforementioned differences, in the current case, both approaches provide similar results, for example, the first solvation shell, identified through the examination of the radial distribution function between pyrimidine center of mass and water center of mass, corresponds well to the first layer described in Ref. [128] and has the same number of coordinated waters (about 21). Nevertheless, the approach employed in this work should be considered generally more accurate, and thus, it is recommended whenever feasible.

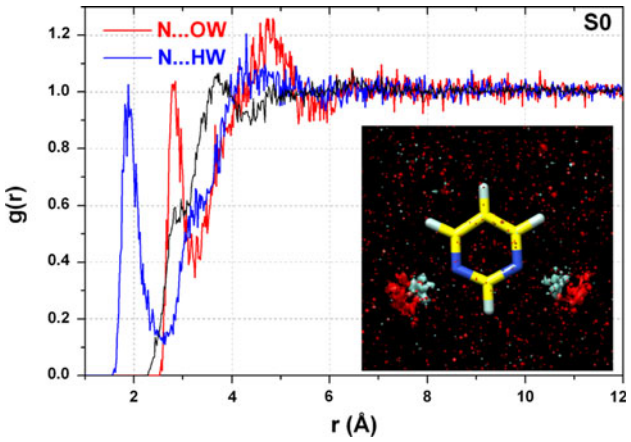

Fig. 9 Radial distribution functions for $N–O_W$ (water oxygen, *red line*), $N–H_W$ (water hydrogen, *blue line*) and $CM_{pyrimidine}$–CM_{H2O} (center of mass of pyrimidine–center of mass of water, *black line*) and three-dimensional contour plots of oxygen (*red*) and hydrogen (*cyan*) densities around pyrimidine

3.6.2 CCl_4

The distribution of CCl_4 solvent molecules around pyrimidine is quite different from water organization. Indeed, CCl_4 molecules have been found at larger distances and their interactions with the solute are weaker. This behavior is clearly depicted in Fig. 10, where both the radial and spatial distribution functions are displayed. The RDF trend shows the presence of three shells, which can be identified with the small peaks centered at about 3.6 Å, 4.8 Å and the broader dominant peak centered at about 6.1 Å. The first two peaks are not well separated and together can be used to define the first solvent layer that extends to about 5.4 Å. This shell contains about 17 solvent molecules, whereas the third peak that stretches up to about 7.3 Å is filled with

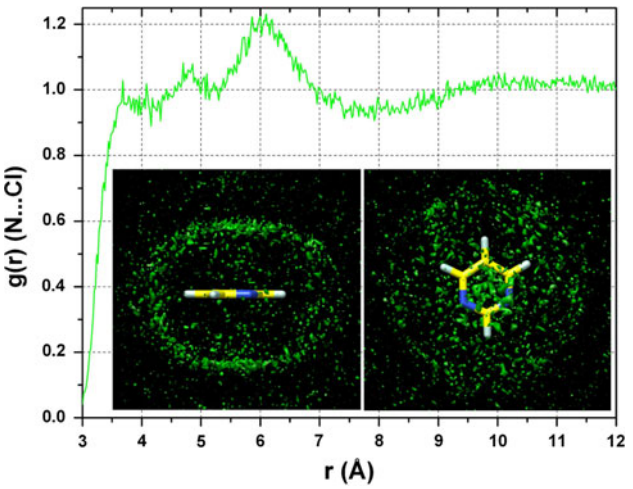

Fig. 10 Radial distribution function in CCl_4 and three-dimensional contour plot of chlorine density around pyrimidine

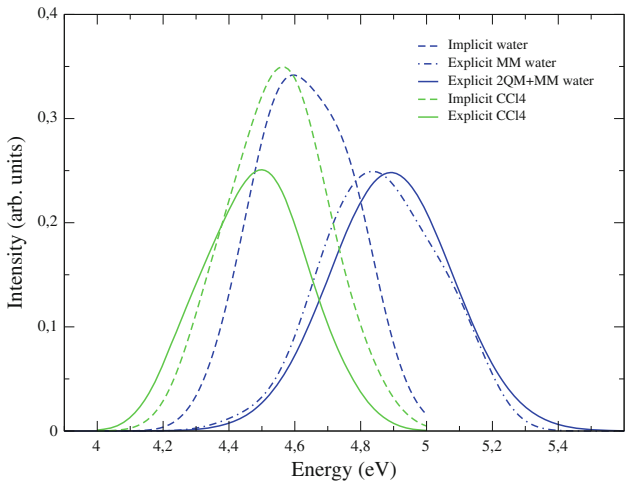

Fig. 11 UV-vis absorption spectra of pyrimidine in water (*blue lines*) and carbon tetrachloride (*green lines*), computed within a time-dependent approach, with implicit (*dashed lines*) and explicit (*solid* and *dash-dot lines*) solvent representations

about 40 CCl_4 molecules, and the shell contains 47 molecules, on average.

The probability distribution of the solvation number (SI, Figure 5) corresponding to the first and second layer is in line with the RDF data. Moreover, the SDF contour plot clearly supports a picture where pyrimidine seems more confined in the solvent cage and adopts a randomly distributed orientation with its motion rather limited. Similarly to what seen for water as solvent, these results match closely the more approximate models previously applied [128].

3.7 UV-vis spectra from a time-dependent approach

To estimate the improvement that can be achieved with the present multi-level time-dependent protocol, the UV-vis absorption $S_1 \leftarrow S_0$ spectrum has first been computed within a static approach, that is, by considering only the minimum energy geometry, optimized at the CAM-B3LYP level in both water and CCl_4, each represented with an implicit description by means of the nonequilibrium LR-CPCM [41]. The vertical excitation energies computed for water (4.69 eV) and carbon tetrachloride (4.61 eV) show only a small difference: in particular, when compared to the gas-phase VE of 4.55 eV, both values show a solvent blue shift of $\sim$1,100 and $\sim$500 cm^{-1}, for H_2O and CCl_4, respectively. As concerns water, the agreement with experimental data [131] is rather poor, the latter being 2,700 cm^{-1}. The blue shift found for CCl_4 can be compared to that computed by Canuto and coworkers [128], obtained with INDO/CIS calculations on supramolecular clusters extracted from Monte Carlo (MC) simulations ($\sim$100 cm^{-1}), the discrepancy is small and in opposite direction with respect to the results obtained for water.

In the time-dependent approach, dynamical averaging effects are taken into account by computing vertical transition energies and oscillator strengths on one hundred frames extracted from the classical MD simulations in each solvent. Moreover, the solvent description has been improved by explicitly considering all solvent molecules within a selected distance from pyrimidine geometrical center. The resulting spectra, obtained by broadening the vertical energies computed at the geometries extracted from the MD simulations with Gaussian functions with HWHM of 0.1 eV, are reported in Fig. 11.

The energies corresponding to the maximum absorption are 4.84 and 4.50 eV for spectra in H_2O and CCl_4, respectively, yielding to a solvent shift (with respect to the vertical transition energy *in vacuo* of 4.52 eV) of $\sim$2,600 and ~ -160 cm^{-1} for the former and latter solvent, respectively, thus improving the agreement with both the above mentioned experimental [131] and computed [128] values. Note that by treating the two closest hydrogen-bonded water molecules to pyrimidine at the QM level, along with the solute, and the remaining solvent molecules as point charges, the computed maximum absorption peak is found at 4.88 eV (see Fig. 11). The good agreement between the latter result and the previous fully electrostatic embedding (solvent) calculations suggests that the interaction between pyrimidine and water is basically electrostatic in nature. It is worth noting that the agreement with the experimental result (2,700 cm^{-1}) for water solvent is also improved with respect to previous calculations reported in the literature [128, 132] (2,223 cm^{-1} and 2,275 cm^{-1}, in Refs. [128] and [132], respectively).

As far as the absorption in CCl_4 is concerned, because of the weak nonpolar interactions between pyrimidine and the

solvent molecules, it is not surprising that the vertical transition energy is only slightly shifted with respect to the value computed *in vacuo*. Indeed, these considerations, together with the less structured framework arising from the RDF analysis as compared to water, suggest that the explicit solvent model could be abandoned for the more computationally convenient PCM. Conversely, the strong local and specific interactions between pyrimidine and water make such a choice less advisable in this case. To verify this hypothesis, only pyrimidine geometries were extracted from MD frames, thus sampling only solute conformational dynamics (see SI, Figure 3). UV-vis absorption spectra have thereafter been computed on such geometries taking into account implicit solvent effects only, for both solvents. As expected, Fig. 11 shows small difference ($\sim 300\ cm^{-1}$) between implicit and implicit/explicit solvent models for the CCl_4, while larger difference arises in the case of water (blue shift of $\sim 700\ cm^{-1}$).

In view of the negligible specific solute–solvent interactions for the CCl_4 solution, time-dependent results computed with solvent modeled by PCM can be directly compared with their time-independent counterparts (SI, Figure 6), with both approaches agreeing on maxima positions and the width of the low-resolution spectra. It must be recalled that the presented approaches allow to study in detail different effects influencing solvent shift and electronic band shape: the former permits to take into account specific and bulk solute–solvent interactions, while the latter allows to analyze individual vibronic contributions. The good overall agreement on the final results confirms that integrated studies, which take advantage of both time-dependent and time-independent approaches, pave the route toward a better understanding of experimentally observed spectra in condensed phases.

4 Conclusions

Some of the most recent theoretical approaches, with particular focus on those either developed or extended and validated by Vincenzo Barone and co-workers, have been presented taking as an example a medium-sized molecule, pyrimidine. We first determined the structure and vibrational properties of the isolated molecule at the CCSD(T) level, while the energies and oscillator strengths of electronic excited states have been characterized at the MRPT level. It has been shown that the DFT method provides accurate results at a relatively low computational cost compared to the wavefunction-based methods that take into account electron correlation (CCSD(T) and MRPT). This allowed us to use hybrid methods, which combine the harmonic force field obtained at the CCSD(T) with the anharmonic corrections at the DFT level, to simulate the vibrational spectrum in good agreement with experiment. Moreover, DFT-based approaches have also been coupled with the PCM method to study the solvent effect on the calculation of anharmonic frequencies in an implicit way. While the $S_1 \leftarrow S_0$ electronic transition of pyridine is not a simple case for the time-independent approaches, which have been employed to simulate vibrationally resolved one-photon absorption and resonance Raman spectra, we have shown how a careful study allows to obtain accurate spectra and to interpret experimental data. Furthermore, the UV-vis electronic spectrum encompassing the first twelve excited electronic states has been computed, showing feasibility of spectra line-shape simulations even in the broad energy range.

Finally, a purposely DFT-tailored force field allowed us to study the conformational flexibility, solvation properties and their influence on the absorption spectrum of pyrimidine. The absorption spectra in water and CCl_4, obtained from several QM/MM/PCM calculations on sampled molecular configurations, have shown a solvatochromic shift in good agreement with experimental data, provided that the solvent is treated explicitly, thus validating the accuracy of the proposed method. In conclusion, we can point out that, although further developments are clearly needed, the accuracy of the computed IR and UV–vis spectra already allows a direct comparison with measurements in solution, and the QM/MM simulations represent a valuable complement to experimental results. This also represents a critical first step to study larger and more complex systems for which high-level theoretical data are unavailable and experimental data may be scarce.

Acknowledgments All authors are grateful to Professor Vincenzo Barone for fruitful collaborations, scientific advices and/or tutoring over the years. This work was supported by Italian MIUR (PRIN2008, PRIN2009). The large scale computer facilities of the VILLAGE network (http://m3village.sns.it) are acknowledged for providing computer resources. The COST-CMTS Action CM1002 "COnvergent Distributed Environment for Computational Spectroscopy (CODECS)" is also acknowledged.

References

1. Laane J (ed) (2009) Frontiers of molecular spectroscopy. Elsevier, Amsterdam
2. Quack M, Merkt F (eds) (2011) Handbook of high-resolution spectroscopy. Wiley, New Jersey
3. Siebert F, Hildebrandt P (eds) (2008) Vibrational spectroscopy in life science. Wiley-VCH Verlag GmbH and Co., KGaA, New Jersey
4. Astrid G, Rudolf R, Jerker W (eds) (2010) Single molecule spectroscopy in chemistry, physics and biology: nobel symposium. Springer,
5. Jensen P, Bunker PR (eds) (2000) Computational molecular spectroscopy. Wiley, New Jersey

6. Barone V (ed) (2011) Computational strategies for spectroscopy, from small molecules to nano systems. Wiley, New Jersey
7. Grunenberg J (ed) (2010) Computational spectroscopy. Wiley-VCH Verlag GmbH & Co., KGaA, New Jersey
8. Pedone A, Biczysko M, Barone V (2010) Chem Phys Chem 11:1812
9. Barone V, Biczysko M, Brancato G (2010) Adv Quantum Chem 59:17
10. Csaszar AG, Fabri C, Szidarovszky T, Matyus E, Furtenbacher T, Czako G (2012) Phys Chem Chem Phys 14:1085
11. Tennyson J (2011) WIREs Comput Mol Sci. doi:10.1002/wcms.94
12. Puzzarini C, Stanton J, Gauss J (2010) Int Rev Phys Chem 29:273
13. Carrington T, Wang XG (2011) WIREs Comput Mol Sci 1:952
14. Csaszar AG (2011) WIREs Comput Mol Sci. doi:10.1002/wcms.75
15. Clary D (2006) Science 314:5797
16. Truhlar DG (2008) J Am Chem Soc 130:16824
17. Visscher L, Bolhuis P, Bickelhaupt FM (2011) Phys Chem Chem Phys 13:10399
18. Pedone A, Prampolini G, Monti S, Barone V (2011) Chem Mater 23:5016
19. Riley KE, Pitonak M, Jurecka P, Hobza P (2010) Chem Rev 110:5023
20. Puzzarini C, Biczysko M, Barone V (2010) J Chem Theory Comput 6:828
21. Barone V, Bloino J, Biczysko M, Santoro F (2009) J Chem Theory Comput 5:540
22. Barone V, Cacelli I, Ferretti A, Prampolini G (2009) J Chem Phys 131:224103
23. Gordon MS, Fedorov DG, Pruitt SR, Slipchenko LV (2012) Chem Rev 112:632
24. Maple J, Dinur U, Hagler A (1988) Proc Natl Acad Sci USA 85:5350
25. Dasgupta S, Yamasaki T, Goddard W III (1996) J Chem Phys 104:2898
26. Cacelli I, Prampolini G (2007) J Chem Theory Comput 3:1803
27. Gao J (1996) Acc Chem Res 29:298
28. Canuto S, Coutinho K, Trzesniak D (2002) New developments in Monte Carlo/quantum mechanics methodology. The solvatochromism of carotene in different solvents. In: Sabin JR, Brandas E (eds) Advances in quantum chemistry, vol 41. Academic Press, pp 161–183
29. Miertus S, Scrocco E, Tomasi J (1981) Chem Phys 55:117
30. Cramer CJ, Truhlar DG (1999) Chem Rev 99:2161
31. Tomasi J, Mennucci B, Cammi R (2005) Chem Rev 105:2999
32. Tomasi J (2011) WIREs Comput Mol Sci 1:855
33. Klamt A (2011) WIREs Comput Mol Sci 1:699
34. Caricato M, Mennucci B, Scalmani G, Trucks GW, Frisch MJ (2010) J Chem Phys 132:084102
35. Improta R, Barone V, Santoro F (2007) Angew Chem Int Ed Engl 46:405
36. Wang YH, Halik M, Wang CK, Marder SR, Luo Y (2005) J Chem Phys 123:194311
37. Mennucci B, Cappelli C, Guido CA, Cammi R, Tomasi J (2009) J Phys Chem A 113:3009
38. Avila Ferrer F, Improta R, Santoro F, Barone V (2011) Phys Chem Chem Phys 13:17007
39. Cammi R, Tomasi J (1995) Int J Quantum Chem: Quantum Chem Symp 29:465
40. Mennucci B, Cammi R, Tomasi J (1998) J Chem Phys 109:2798
41. Marenich AV, Cramer CJ, Truhlar DG, Guido CA, Mennucci B, Scalmani G, Frisch MJ (2011) Chem Sci 2:2143
42. Rivail JL, Rinaldi D, Dillet V (1996) Mol Phys 89:1521
43. Cappelli C (2007) Continuum solvation approaches to vibrational properties. In: Mennucci B, Cammi R (eds) Continuum solvation models in chemical physics: theory and applications. Wiley, Chichester, p 167
44. Cappelli C, Biczysko M (2011) Time-independent approach to vibrational spectroscopies. In: Barone V (ed) Computational strategies for spectroscopy. Wiley, pp 309–360
45. Bandyopadhyay P, Gordon MS (2000) J Chem Phys 113:1104
46. Mennucci B, Martinez JM, Tomasi J (2001) J Phys Chem A 105:7287
47. Barone V, Improta R, Rega N (2008) Acc Chem Res 41:605
48. Cappelli C, Mennucci B, da Silva CO, Tomasi J (2000) J Chem Phys 112:5382
49. Santoro F, Barone V, Gustavsson T, Improta R (2006) J Am Chem Soc 128:16312
50. Gao J, Truhlar DG (2002) Annu Rev Phys Chem 53:467
51. Brancato G, Rega N (2011) Computational spectroscopy by classical time-dependent approaches. In: Barone V (ed) Computational strategies for spectroscopy. Wiley, pp 517–547
52. Biczysko M, Bloino J, Santoro F, Barone V (2011) Time-independent approaches to simulate electronic spectra lineshapes: from small molecules to macrosystems. In: Barone V (ed) Computational strategies for spectroscopy. Wiley, pp 361–443
53. Grimme S (2004) Calculation of the electronic spectra of large molecules. In: Reviews in computational chemistry. Wiley, pp 153–218
54. Cui Q, Karplus M (2000) J Chem Phys 112:1133
55. Aidas K, Mikkelsen KV, Kongsted J (2007) J Comp Methods Sci Eng 7:135
56. Barone V, Polimeno A (2007) Chem Soc Rev 36:1724
57. Ramos MJ (ed) (2008) Computational proteomics. Transw Res Netw
58. Grotendorst J, Attig N, Blügel S, Marx D (eds) (2009) Multiscale simulation methods in molecular sciences. Lecture Notes, NIC Series:42
59. Senn HM, Thiel W (2009) Angew Chem Int Ed Engl 48:1198
60. Sabin, JR, Brandas, E (eds) (2010) Advances in quantum chemistry, vol 59. Academic Press, Massachusetts
61. Arul Murugan N, Kongsted J, Rinkevicius Z, Aidas K, Ågren H (2010) J Phys Chem B 114:13349
62. Raghavachari K, Trucks GW, Pople JA, Head-Gordon M (1989) Chem Phys Lett 157:479
63. Helgaker T, Klopper W, Koch H, Noga J (1997) J Chem Phys 106:9639
64. CFOUR, a quantum chemical program package written by Stanton JF, Gauss J, Harding ME, Szalay PG with contributions from A.A. Auer, R.J. Bartlett, U. Benedikt, C. Berger, D.E. Bernholdt, Y.J. Bomble, L. Cheng, O. Christiansen, M. Heckert, O. Heun, C. Huber, T.-C. Jagau, D. Jonsson, J. Jusélius, K. Klein, W.J. Lauderdale, D.A. Matthews, T. Metzroth, L.A. Mück, D.P. O'Neill, D.R. Price, E. Prochnow, C. Puzzarini, K. Ruud, F. Schiffmann, W. Schwalbach, S. Stopkowicz, A. Tajti, J. Vázquez, F. Wang, J.D. Watts and the integral packages MOLECULE (J. Almlöf and P.R. Taylor) PROPS (P.R. Taylor) ABACUS (T. Helgaker, H.J. Aa. Jensen, P. Jørgensen, and J. Olsen) and ECP routines by A. V. Mitin and C. van Wüllen. For the current version, see http://www.cfour.de
65. Huron B, Malrieu JP, Rancurel P (1973) J Chem Phys 58:5745
66. Angeli C, Cimiraglia R, Persico M, Toniolo A (1997) Theor Chem Acc 93:57
67. Angeli C, Persico M (1997) Theor Chem Acc 98:117
68. Barone V, Cimino P, Stendardo E (2008) J Chem Theory Comput 4:751
69. Barone V, Bloino J, Biczysko M (2010) Phys Chem Chem Phys 12:1092
70. Becke AD (1993) J Chem Phys 98:5648
71. Yanai T, Tew DP, Handy NC (2004) Chem Phys Lett 393:51
72. Grimme S (2006) J Chem Phys 124:034108

73. Double and triple-ζ basis sets of n07 family, are available for download. Visit http://idea.sns.it (Accessed June 30, 2011)
74. Frisch MJ, Trucks GW, Schlegel HB, Scuseria GE, Robb MA, Cheeseman JR, Scalmani G, Barone V, Mennucci B, Petersson GA, Nakatsuji H, Caricato M, Li X, Hratchian HR, Izmaylov AF, Bloino J, Zheng G, Sonnenberg JL, Hada M, Ehara M, Toyota K, Fukuda R, Hasegawa J, Ishida M, Nakajima T, Honda Y, Kitao O, Nakai H, Vreven T, Montgomery Jr. JRJ. A. Peralta, Ogliaro F, Bearpark M, Heyd JJ, Brothers E, Kudin KN, Staroverov VN, Kobayashi R, Normand J, Raghavachari K, Rendell A, Burant JC, Iyengar SS, Tomasi J, Cossi M, Rega N, Millam JM, Klene M, Knox JE, Cross JB, Bakken V, Adamo C, Jaramillo J, Gomperts R, Stratmann RE, Yazyev O, Austin AJ, Cammi R, Pomelli C, Ochterski JW, Martin RL, Morokuma K, Zakrzewski VG, Voth GA, Salvador P, Dannenberg JJ, Dapprich S, Daniels AD, Farkas O, Foresman JB, Ortiz JV, Cioslowski J, Fox DJ, Gaussian 09 Revision B.01 (2009) Gaussian Inc. Wallingford CT 2009
75. Brancato G, Rega N, Barone V (2008) J Chem Phys 128:144501
76. Brancato G, Rega N, Barone V (2009) Chem Phys Lett 483:177
77. van der Spoel D, Lindahl E, Hess B, Groenhof G, Mark A, Barendsen H (2005) J Comp Chem 26:1701
78. Brancato G (2011) Jersey—a multi-purpose molecular simulation program
79. van der Spoel D, Lindahl E, Hess B, Buuren Avan, Apol E, Meulenhoff P, Tieleman D, Sijbers A, Feenstra K, Drunen Rvan, Berendsen H (2010) Gromacs user manual version, 4.5.4 http://www.gromacs.org
80. Mills IM (1972) Molecular spectroscopy: modern research. Academic Press, New York
81. Truhlar DG, Olson RW, Jeannotte AC II, Overend J (1976) J Am Chem Soc 98:2373
82. Isaacson AD, Truhlar DG, Scanlon K, Overend J (1981) J Chem Phys 75:3017
83. Amos RD, Handy NC, Green WH, Jayatilaka D, Willets A, Palmieri P (1991) J Chem Phys 95:8323
84. Gaw F, Willetts A, Handy N, Green W (1991) SPECTRO—a program for derivation of spectroscopic constants from provided quartic force fields and cubic dipole fields. In: Bowman JM (ed) Advances in molecular vibrations and collision dynamics, vol 1B. JAI Press, pp 169–185
85. Zhang Q, Day PN, Truhlar DG (1993) J Chem Phys 98:4948
86. Vazquez J, Stanton JF (2006) Mol. Phys. 104:377
87. Barone V (2005) J Chem Phys 122:014108
88. Barone V (2004) J Chem Phys 120:3059
89. Bloino J, Guido C, Lipparini F, Barone V (2010) Chem Phys Lett 496:157
90. Carbonniere P, Lucca T, Pouchan C, Rega N, Barone V (2005) J Comp Chem 26:384
91. Begue D, Benidar A, Pouchan C (2006) Chem Phys Lett 430:215
92. Cappelli C, Monti S, Scalmani G, Barone V (2010) J Chem Theory Comput 6:1660
93. Cappelli C, Lipparini F, Bloino J, Barone V (2011) J Chem Phys 135:104505. Erratum ibidem 2011, 135, 149901
94. Cappelli C, Corni S, Cammi R, Mennucci B, Tomasi J (2000) J Chem Phys 113:11270
95. Cammi R, Cappelli C, Corni S, Tomasi J (2000) J Phys Chem A 104:9874
96. Bloino J, Biczysko M, Santoro F, Barone V (2010) J Chem Theory Comput 6:1256
97. Santoro F, Cappelli C, Barone V (2011) J Chem Theory Comput 7:1824
98. Santoro F *FCclasses*, a fortran 77 code (2008) Available via the Internet at http://village.pi.iccom.cnr.it; last accessed July 14, 2011
99. Santoro F, Improta R, Lami A, Bloino J, Barone V (2007) J Chem Phys 126:084509
100. Dierksen M, Grimme S (2005) J Chem Phys 122:244101
101. Jankowiak HC, Stuber JL, Berger R (2007) J Chem Phys 127:234101
102. Hazra A, Nooijen M (2003) Int J Quantum Chem 95:643
103. Cossi M, Scalmani G, Rega N, Barone V (2003) J Comp Chem 24:669
104. Cammi R, Corni S, Menucci B, Tomasi J (2005) J Chem Phys 122:104513
105. Corni S, Cammi R, Menucci B, Tomasi J (2005) J Chem Phys 123:134512
106. Scalmani G, Frisch MJ, Menucci B, Tomasi J, Cammi R, Barone V (2006) J Chem Phys 124:094107
107. Kisiel Z, Pszczółkowski L, López J, Alonso J, Maris A, Caminati W (1999) J Mol Spectrosc 195:332
108. Puzzarini C (2009) J Phys Chem A 113:14530
109. Puzzarini C (2010) Int J Quant Chem 110:2483
110. Puzzarini C, Barone V (2011) Phys Chem Chem Phys 13:7158
111. Dunning T Jr (1989) J Chem Phys 90:1007
112. Kendall A, Dunning TH Jr, Harrison RJ (1992) J Chem Phys 96:6796
113. Peach MJG, Helgaker T, Salek P, Keal TW, Lutnaes OB, Tozer DJ, Handy NC (2006) Phys Chem Chem Phys 8:558
114. Silva F Ferreira da, Almeida D, Martins G, Milosavljevic AR, Marinkovic BP, Hoffmann SV, Mason NJ, Nunes NJ, Garcia G, Limao-Vleira G (2010) Phys Chem Chem Phys 12:6717
115. Biczysko M, Panek P, Scalmani G, Bloino J, Barone V (2010) J Chem Theory Comput 6:2115
116. Kozuch S, Gruzman D, Martin JML (2010) 114:20801
117. Martin JML, Lee TJ, Taylor PR, Francois JP (1995) J Chem Phys 103:2589
118. Barone V, Festa G, Grandi A, Rega N, Sanna N (2004) Chem Phys Lett 388:279
119. Barone V (2004) J Phys Chem A 108:4146
120. Boese AD, Martin J (2004) J Phys Chem A 108:3085
121. Breda S, Reva ID, Lapinski L, Nowak MJ, Fausto R (2006) J Mol Struct 786:193
122. Cappelli C, Corni S, Tomasi J (2001) J Chem Phys 115:5531
123. Cappelli C, Corni S, Mennucci B, Cammi R, Tomasi J (2002) J Phys Chem A 106:12331
124. See http://webbook.nist.gov/cgi/cbook.cgi?id=c289952. Last accessed june 23th 2011
125. Hazra A, Nooijen M (2005) Phys Chem Chem Phys 7:1759
126. Lin N, Santoro F, Zhao X, Rizzo A, Barone V (2008) J Phys Chem A 112:12401
127. Lami A, Santoro F (2011) Time-dependent approaches to calculation of steady-state vibronic spectra: from fully quantum to classical approaches. In: Barone V (ed) Computational strategies for spectroscopy. Wiley, pp 475–516
128. de Almeida K, Coutinho K, de Almeida W, Rocha W, Canuto S (2001) Phys Chem Chem Phys 3:1583
129. Barone V, Bloino J, Monti S, Pedone A, Prampolini G (2011) Phys Chem Chem Phys 12:10550
130. Barone V, Bloino J, Monti S, Pedone A, Prampolini G (2011) Phys Chem Chem Phys 13:2160
131. Baba H, Goodman L, Valenti P (1996) J Am Chem Soc 88:5410
132. Gao J, Byun K (1997) Theor Chem Acc 96:151